MIMO-Assisted MPR-Aware MAC Design for Asynchronous WLANs

Sanaz Barghi, *Student Member, IEEE*, Hamid Jafarkhani, *Fellow, IEEE*, and Homayoun Yousefi'zadeh, *Senior Member, IEEE*

***Abstract*—The use of multiple-packet reception (MPR) in wireless networks is known to improve throughput especially in high-traffic conditions. The lack of synchronization among the nodes in random access systems introduces significant challenges toward the adoption of MPR in the PHY and the MAC design for systems using MPR. In this paper, we propose an asynchronous MPR method for the PHY and also design a compatible random access MAC for wireless local area networks (WLANs). Relying on space–time coding techniques, our MPR method detects multiple asynchronous packets while providing diversity and low bit error rates at the PHY layer. Extending the design of IEEE 802.11, our MPR MAC design encourages simultaneous packet transmissions and handles multiple packet receptions. Simulation results show that the throughput of a WLAN significantly improves in many scenarios of operation using our proposed PHY/MAC MPR framework.**

***Index Terms*—Cross-layer design, IEEE 802.11, MAC, multiple-input–multiple-output (MIMO), multiple-packet reception (MPR), space–time code (STC).**

I. Introduction

LAYERED OSI architecture is the *de facto* standard of operation in wired networks. In wired networks, isolated per-layer optimization techniques have been successfully and practically applied to improve network performance. However, applying per-layer optimization techniques is of limited value in wireless networks due to openness of transmission media. Instead, cross-layer optimization techniques have gained widespread use in the wireless network design methodologies. The work of [1] and the references therein describe some of the cross-layer algorithms designed for data-link, network, and transport layers.

MAC protocol design within the data-link layer is traditionally carried independent of the PHY layer. The latter is under the assumption that the PHY layer is incapable of detecting colliding packets, and hence simultaneous transmissions always fail. In reality, multiuser detection (MUD), successive interference cancellation (SIC), and code division multiple access (CDMA) are examples of multiple-packet reception (MPR) techniques by which the PHY layer can detect more than one packet at a time. Hypothetically, detecting two packets at a time can double the throughput of a network. With MPR techniques, collisions are resolved in the PHY as opposed to the MAC layer, and simultaneous transmissions are possible. While resolving collisions at the PHY layer can simplify MAC design, because the PHY can detect a number of simultaneous packet receptions, the MAC is still required to handle higher layer collisions. This will remove the separation of MAC and PHY layers, but allows for enhancing performance.

In practical networks, it is almost impossible to have a fully synchronized reception from physically separated clients. At the very least, an asynchrony in a fraction of a symbol transmission duration is always expected due to different propagation delays. Therefore, MPR methods must detect multiple asynchronous transmissions. Asynchronous MPR methods are mostly complicated. Direct sequence-CDMA (DS-CDMA) is one of the simple asynchronous MPR methods. However, cross-layer design techniques relying on CDMA suffer from exhaustive code search overhead. By assigning codes to different packet types instead of different users, the authors of [2] design a MAC algorithm for multihop *ad hoc* networks. Unfortunately, the power control overhead associated with DS-CDMA reduces the practical value of their algorithm. Under some signal-to-interference-plus-noise ratio (SINR) and timing constraints, the use of the message in message (MIM) scheme [3] enables concurrent transmissions. In [4], the Shuffle Algorithm is proposed to centrally schedule transmissions by different interfering access points (APs). This algorithm takes into account the timing requirements of MIM and schedules transmissions from different APs to comply with that in a manner that enables successful simultaneous transmissions. Another algorithm that targets solving the collision problem in the PHY is ZigZag decoding [5]. Utilizing an iterative algorithm, ZigZag decoding resolves two similar consecutive collisions. Although the algorithm does not require any central decision-making unit, it requires the observation of multiple collisions between two packets before decoding such collided packets.

Other promising simple MPR techniques are those based on multiple-input–multiple-output (MIMO) systems. Switching to higher frequencies increases the feasibility of having multiple-antenna users. Exploiting the benefits of having multiple-antenna nodes in a network has been studied in recent years as described in the works of [6]–[9]. MIMO communications enhance the performance of a wireless communication

Manuscript received November 20, 2009; revised July 21, 2010 and February 21, 2011; accepted March 03, 2011; approved by IEEE/ACM TRANSACTIONS ON NETWORKING Editor S. Kasera. This work was supported in part by the Boeing Company under a grant.

The authors are with the Center for Pervasive Communications and Computing (CPCC), University of California, Irvine, Irvine, CA 92717 USA (e-mail: sbarghi@uci.edu; hamidj@uci.edu; hyousefi@uci.edu).

Color versions of one or more of the figures in this paper are available online at http://ieeexplore.ieee.org.

Digital Object Identifier 10.1109/TNET.2011.2130538

system in a number of different ways. The available diversity gain with space–time codes (STCs) enhances the link quality and can be used to increase the data rate by means of using denser signal constellations [10]. By spatial multiplexing, for example using V-BLAST [11], several parallel independent data streams can be sent simultaneously to increase the throughput. Beamforming concentrates the transmission energy in one direction in order to increase signal-to-noise ratio (SNR) and range. On the other hand, interference nulling prevents reception from a certain direction and reduces the level of interference sensed from other transmissions. Recently, MPR methods have been developed for MIMO systems. For example, transmit antennas are not required to be on a single node in order for a V-BLAST receiver to work [7]. Therefore, multiple streams of data coming from different sources can be separated at a multiple-antenna receiver. An MPR method based on STC is also developed in [12] for two users with two transmit antennas. Independent space–time coded streams are separable at a multiple-antenna receiver by preserving some degree of diversity. In [13], the work is generalized to the case of multiple users with a higher number of antennas.

This study is not the first study focusing on cross-layer MIMO-MPR design. The authors of [7] design a MAC for WLANs without hidden terminals. The MAC algorithm is the same as IEEE 802.11 with RTS/CTS signaling [14], except that it has additional receiver address fields in CTS and ACK frames to grant permission for the transmission of more than one node at a time. The design assumes that all nodes are single-antenna nodes, and a multiple-antenna AP utilizes an MUD method to detect different data streams. However, the major drawback of the design is that it completely ignores the hidden-terminal problem. More importantly, the MPR method cannot achieve good bit error rate (BER) performance and loses diversity as the number of streams to be decoded increases. When the MPR method has a high BER, long data packets will be dropped with a high probability because of the error. This degrades the throughput of the MPR system in comparison to traditional systems. The latter is due to the fact that the overhead is in the order of long data packets, as opposed to short RTS packets wasted by collisions. An important benefit of employing STC-based MPR is providing a high diversity order compared to other MIMO-MPR methods.

The authors of [15] introduce an MPR-aware MAC for a WLAN based on slotted ALOHA. The PHY-layer design is a combination of spatial multiplexing and STC-based MPR. All nodes as well as the AP are two-antenna nodes. In this method, each packet is broken into two equal-length sections and sent through each antenna. The AP examines the received signal in order to find the number of simultaneously received packets. For single-packet receptions, V-BLAST is used. For double-packet receptions, a retransmission follows, and STC-based MPR is employed. While this MPR-aware MAC improves the performance in comparison to slotted ALOHA, it yet again ignores the problem of hidden terminals and further assumes the nodes to be perfectly synchronized.

In this paper, an MPR method based on the use of STC is introduced. Along with providing a high diversity, the method detects clock and frequency asynchrony of transmissions. Being able to work with asynchronous packets reduces the synchronization signaling overhead in the network and also allows the MAC algorithm to properly handle the hidden-terminal problem. The MPR-aware MAC algorithm introduced in this paper is designed for WLANs with and without hidden terminals. Each packet is vulnerable to collisions for a duration twice its length. Although RTS/CTS signaling is designed to combat the collision problem, the problem could still drastically lessen the throughput and significantly increase the delay of an 802.11 network. The MPR-aware MAC algorithm of this paper is designed to accommodate as many simultaneous transmissions as the maximum number of packets decodable by the PHY.

Based on the review of the literature work in this area, the main contributions of this paper are threefold. First, it is apparent that all works utilizing STC-based MPR have only been operational under near-perfect synchronization assumptions. While other works depending on BLAST-like MPR do not require symbol synchronization, they are characterized by high bit error rates when detecting multiple packets. To the best of our knowledge, this paper introduces the first asynchronous STC-based MPR framework that is capable of preserving diversity gain even when packets are asynchronous. Second, none of the previously proposed MIMO-MPR cross-layer designs have considered the impact of hidden terminals. Unlike previous designs, the proposed design of this paper considers the issue of hidden terminals. Third, previous designs have ignored the fact that network throughput can be improved by increasing the number of multiple transmissions. Contrary to the previous design work, the current design encourages a higher number of multiple packet transmissions and employs a new MAC design capable of improving network throughput.

The rest of this paper is organized as follows. In Section II, the operation of the MPR method in the PHY layer is described. In Section III, our MPR-aware MAC algorithm based on the IEEE 802.11 standard is discussed. Section IV presents the throughput analysis for a network of two hidden nodes when the proposed MPR-aware MAC algorithm is utilized. In Section V, extensive analysis and simulation results are presented to illustrate the benefits of our MPR system. Finally, Section VI concludes the paper.

II. Physical-Layer Model

It is well understood that distributed nodes typically do not agree on their clock and central frequency. Exchanging time-stamped packets is one of the most practical synchronization methods for affine clocks. In [16], the authors show that it is not possible to perfectly estimate all affine clock parameters even in a noise-free environment, and there is always some level of deviation between such parameter estimations. Clock skews can be adjusted, resulting in equal-length symbols while clock offsets may vary. Furthermore, there is a frequency offset between the receiver and the transmitter that is typically estimated such that the associated effect can be canceled in the demodulation blocks. It is also important to note that some advanced synchronization techniques such as timing advance in 3GPP long-term evolution (LTE) [17] are able to compensate for the asynchrony of sources. However, such methods typically have an accuracy

limitation preventing them from achieving exact synchronization between multiple packet receptions. In addition, the use of cyclic prefix (CP) within OFDMA symbols takes care of the remaining asynchrony for as long as the asynchrony between the two packets is less than the length of the CP. To the contrary, our paper focuses on time-domain solutions for systems such as random access WLANs. The latter systems are characterized by the fact that they have a low synchronization overhead, use non-OFDM modulation schemes, and impose no restriction on the asynchrony level between the two received packets.

Since multiple packets reaching a receiver never agree on their time and frequency offsets, MPR methods need to handle detection of asynchronous packets. In what follows, we generalize the STC-based MPR methods in [12] and [13] for detecting asynchronous space–time coded packets.

A. Channel Model

In our paper, a quasi-static Rayleigh flat fading channel model is employed where channel coefficients are assumed to be constant during the transmission period of a packet. Channel coefficients are assumed to be i.i.d. complex Gaussian random variables. The channel coefficient from the transmitter's nth antenna to the receiver's mth antenna is denoted by $\alpha_{n,m}$.

Let $C_n(t) = \sum_{l=1}^{L} s_n^l p(t - lT_s)$ be the transmitted signal from Antenna n, where s_n^l is the lth transmitted symbol and $p(t)$ is the impulse response of the pulse shaping filter. Furthermore, let $r_m(kT_s)$ be the received signal sampled at $t = kT_s$ at Antenna m. The samples of the received signal are expressed as

$$r_m(kT_s) = \sum_{n=1}^{N} \alpha_{n,m} \sum_{l=1}^{L} s_n^l P(kT_s + \epsilon T_s - lT_s) e^{j2\pi k \delta f T_s} + \eta_{n,m} \quad (1)$$

where sampling error $-1/2 < \epsilon < 1/2$ is a function of clock offsets as well as propagation delay between the transmitter and the receiver, $P(t)$ is the impulse response of the pulse shaping filter after passing through the receiver filter, and δf is the frequency difference between the transmitter and the receiver.

B. Time Synchronization

Imperfect sampling means that the receiver cannot correctly compensate for imperfections such as different clock offsets and propagation delay. Since an imperfect sampler samples $P(t)$ at some time other than kT_s, not only is the kth sample of the received signal $r_m(kT_s)$ a function of the kth transmitted symbols s_n^ks, but it is also a function of the neighboring symbols, $\ldots, s_n^{k-2}, s_n^{k-1}, s_n^{k+1}, s_n^{k+2}, \ldots$. This effect is called intersymbol interference (ISI). Receivers should estimate the optimum sampling time and track it during decoding in order to eliminate the ISI effect.

Consider a case in which a number of asynchronous terminals are simultaneously transmitting to a single receiver. Each transmitter has a unique clock offset and propagation delay with respect to the receiver. Even if the receiver is capable of sampling the received signal perfectly, sampling a superposition of asynchronous signals cannot be perfect for more than one of them. In this case, multiuser detection methods designed for synchronized transmitters may fail to perform as expected. For example, the array processing method of [12] loses diversity when transmitters are not synchronized. Fig. 1 compares the BER performance of this method for synchronous and asynchronous cases utilizing two-antenna terminals. Note that in Fig. 1, even time differences as small as 5% of a symbol duration result in the loss of diversity. The loss of diversity gain is equal to a higher BER and, in turn, a higher packet error rate (PER). It is important to note that an MPR-aware MAC algorithm is more sensitive to the BER of the PHY compared to a standard MAC algorithm. For example, the time wasted due to a packet collision for standard IEEE 802.11 with RTS/CTS signaling is $\mathrm{RTS} + \mathrm{SIFS} + \mathrm{CTS}$, while the same collision leads to a time wastage of $\mathrm{RTS}{+}\mathrm{SIFS}{+}\mathrm{CTS}{+}\mathrm{SIFS}{+}\mathrm{DATA}{+}\mathrm{SIFS}{+}\mathrm{ACK}$ for an MPR method, which is much longer. Thus, packet loss in MPR-aware networks can undesirably lower the throughput.

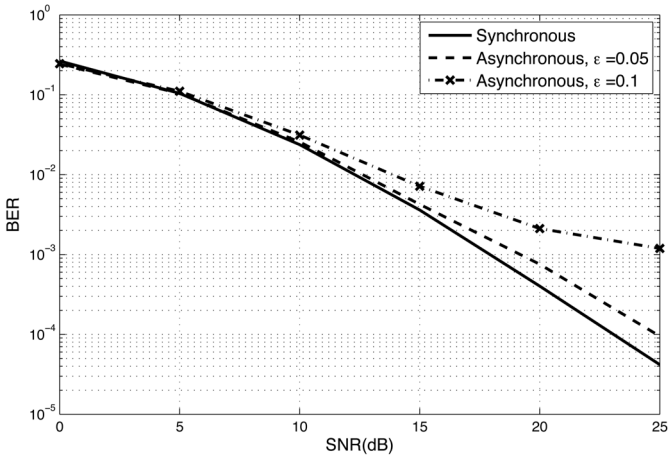

Fig. 1. Performance of the method of [12] for an asynchronous transmission, a 2×2 link, and QPSK modulation.

In what follows, we introduce a transmission scheme that provides the promised diversity of [12] even when transmitters are not synchronized. For the sake of discussion, let all terminals be two-antenna terminals. This method can be easily expanded to the case of terminals with more than two antennas. First, let us explain the details of an array processing technique to detect multiple symbol-synchronous transmissions. Terminals employ Alamouti coding [18] to encode and transmit symbols s_1 and s_2 as follows:

$$C = \begin{pmatrix} s_1 & s_2 \\ -s_2^* & s_1^* \end{pmatrix}. \quad (2)$$

A two-antenna receiver can at most decode two simultaneous signals. Suppose Terminal j transmits $s_k(j)$. The received signal at the mth antenna of the receiver can be written as

$$\begin{pmatrix} R_{1,m} \\ R_{2,m}^* \end{pmatrix} = \begin{pmatrix} \alpha_{1,m}(1) & \alpha_{2,m}(1) \\ \alpha_{2,m}^*(1) & -\alpha_{1,m}^*(1) \end{pmatrix} \cdot \begin{pmatrix} s_1(1) \\ s_2(1) \end{pmatrix} + \begin{pmatrix} \alpha_{1,m}(2) & \alpha_{2,m}(2) \\ \alpha_{2,m}^*(2) & -\alpha_{1,m}^*(2) \end{pmatrix} \cdot \begin{pmatrix} s_1(2) \\ s_2(2) \end{pmatrix} + \begin{pmatrix} \eta_{1,m} \\ \eta_{2,m}^* \end{pmatrix}. \quad (3)$$

Let us denote the matrix multiplied by $(s_1(j)\, s_2(j))^T$ in (3) as $\mathbf{A}_m(j)$. Then, $\mathbf{A}_m(j)$ is a multiple of a unitary matrix. To cancel out the interference from Terminal 2, $R_m = (R_{1,m}\ R_{2,m}^*)^T$ is multiplied by $\mathbf{A}_m^{\mathrm{H}}(2)$ and divided by $|\mathbf{A}_m(2)|^2 = |\alpha_{1,m}(2)|^2 +$

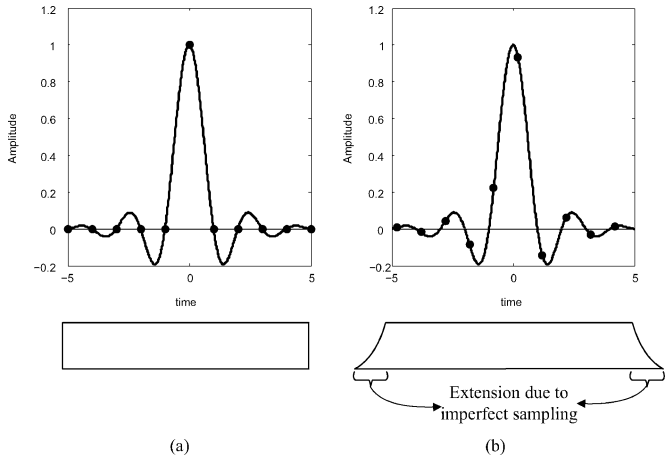

Fig. 2. Effect of (a) perfect and (b) imperfect sampling.

$|\alpha_{2,m}(2)|^2$, where $(\cdot)^{\mathrm{H}}$ is the Hermitian transpose of a matrix. Then, subtracting the samples of the first antenna from those of the second antenna results in

$$\frac{\mathbf{A}_2^{\mathrm{H}}(2)R_2}{|\mathbf{A}_2(2)|^2}-\frac{\mathbf{A}_1^{\mathrm{H}}(2)R_1}{|\mathbf{A}_1(2)|^2} = \left(\frac{\mathbf{A}_2^{\mathrm{H}}(2)\mathbf{A}_2(1)}{|\mathbf{A}_2(2)|^2}-\frac{\mathbf{A}_1^{\mathrm{H}}(2)\mathbf{A}_1(1)}{|\mathbf{A}_1(2)|^2}\right)\begin{pmatrix}s_1(1)\\ s_2(1)\end{pmatrix}+\begin{pmatrix}\eta'_{1,m}\\ \eta'^{*}_{2,m}\end{pmatrix}. \tag{4}$$

In (4), the matrix multiplied by the signal vector is a multiple of a unitary matrix, and decoding the data of the first terminal using (4) is straightforward. This array processing technique provides a diversity of degree 2 for each terminal.

Now, we present our new transmission method that works after relaxing the synchronization assumption. To transmit a packet of $2M$ symbols, i.e., $s_1, s_2, \ldots, s_{2M-1}, s_{2M}$, each transmitter forms two super-symbols, namely S_1 and S_2, as

$$\begin{aligned} S_1 &= (s_1, s_2, \ldots, s_M)\\ S_2 &= (s_{M+1}, s_{M+2}, \ldots, s_{2M}). \end{aligned} \tag{5}$$

Then, each terminal transmits according to the Alamouti coding scheme of (2) while replacing symbols s_j with super-symbols S_j. The transmitter sends M symbols of super-symbols S_1 and S_2 in the first transmission interval from its first and second antenna, respectively. During the second transmission interval, the transmitter sends $-S_2^*$ and S_1^* from the first and the second antenna, respectively.

Due to finite impulse response (FIR) implementation of the pulse shaping filters, each symbol will cause ISI to its nearest neighbors in the case of imperfect synchronization. The effect of sampling error on the received signal is illustrated in Fig. 2. We note that perfect sampling, Fig. 2(a), does not cause ISI while imperfect sampling, Fig. 2(b), causes ISI and expands the received packet. As illustrated by Fig. 2, an imperfectly sampled super-symbol is expanded at its two ends in comparison to a perfectly sampled super-symbol. Let us assume that the FIR pulse shaping filter expands a super-symbol by l, for example $l = 5$, symbols. If the transmitted super-symbol is the

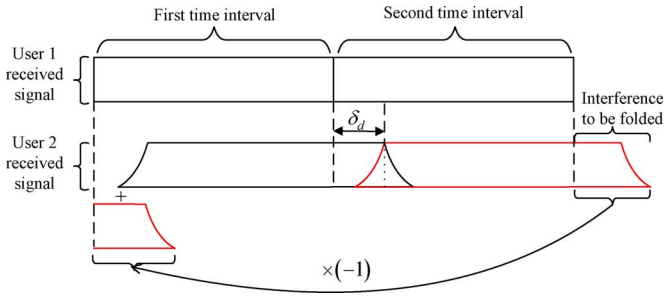

Fig. 3. Diagram of noiseless received signals at the receiver and the interference folding process.

row vector S_j, the expanded super-symbol after imperfect sampling of ϵ is given by the following equation:

$$\tilde{S}_j = (0\,0\,0\,0\,0\,S_j\,0\,0\,0\,0\,0)\times\mathbf{F}^T$$
$$\mathbf{F} = \begin{pmatrix} P_0 & P_{-1} & P_{-2} & \cdots & P_{-(L+2l)}\\ P_1 & P_0 & P_{-1} & \cdots & P_{-(L+2l-1)}\\ \vdots & & & \ddots & \\ P_{L+2l} & P_{L+2l-1} & P_{L+2l-2} & \cdots & P_0 \end{pmatrix} \tag{6}$$

where $P_k = P(\epsilon T_s + kT_s)$.

Now, consider two terminals transmitting according to the above transmission scheme. The noiseless received signals from two transmitters arriving with a time difference of δ_d at the receiver are shown in Fig. 3. Without loss of generality, we assume that the signal of Terminal 1 is sampled perfectly and the signal of Terminal 2 is sampled with a sampling error of ϵ.

Fig. 3 illustrates that when signals from different users reach a destination with a time delay, the interference is asymmetric over the two sections of the desired signal. Fig. 3 also depicts that the received signal is "folded" on itself and multiplied by a factor of -1 in order to generate the symmetric Alamouti structure for the interference. The following equations explain the folding process:

If $d > l$

$$\begin{aligned}\mathcal{S}_1 = \Big(&\tilde{S}_2^*[M+l-d+1], \tilde{S}_2^*[M+l-d+2], \ldots,\\ &\tilde{S}_2^*[M], \tilde{S}_2^*[M+1]+\tilde{S}_1[1], \ldots, \tilde{S}_2^*[M+2l]\\ &+\tilde{S}_1[2l], \tilde{S}_1[2l+1], \ldots, \tilde{S}_1[M+2l-d]\Big)\\ \mathcal{S}_2 = \Big(&-\tilde{S}_1^*[M+l-d+1], -\tilde{S}_1^*[M+l-d+2], \ldots,\\ &-\tilde{S}_1^*[M], -\tilde{S}_1^*[M+1]+\tilde{S}_2[1], \ldots, -\tilde{S}_1^*[M+2l]\\ &+\tilde{S}_2[2l], \tilde{S}_2[2l+1], \ldots, \tilde{S}_2[M+2l-d]\Big).\end{aligned}$$

If $d \le l$

$$\begin{aligned}\mathcal{S}_1 = \Big(&\tilde{S}_2^*[M+l-d+1]+\tilde{S}_1[l-d+1], \ldots,\\ &\tilde{S}_2^*[M+2l]+\tilde{S}_1[2l], \tilde{S}_1[2l+1], \tilde{S}_1[2l+2], \ldots,\\ &\tilde{S}_1[M], \tilde{S}_1[M]-\tilde{S}_2^*[1], \ldots,\\ &\tilde{S}_1[M+l-d]-\tilde{S}_2^*[l-d]\Big)\end{aligned}$$

$$\mathcal{S}_2 = \Big(\tilde{S}_2[l-d+1] - \tilde{S}_1^*[M+l-d+1], \ldots, \tilde{S}_2[2l] - \tilde{S}_1^*[M+2l], \tilde{S}_2[2l+1], \tilde{S}_2[2l+2], \ldots, \tilde{S}_2[M], \tilde{S}_1^*[1] + \tilde{S}_2[M], \ldots, \tilde{S}_1^*[l-d] + \tilde{S}_2[M+l-d]\Big).$$

Therefore, we have

$$\begin{pmatrix} R_{1,m} \\ R_{2,m}^* \end{pmatrix} = \begin{pmatrix} \alpha_{1,m}(1) & \alpha_{2,m}(1) \\ \alpha_{2,m}^*(1) & -\alpha_{1,m}^*(1) \end{pmatrix} \cdot \begin{pmatrix} S_1(1) \\ S_2(1) \end{pmatrix} + \begin{pmatrix} \alpha_{1,m}(2) & \alpha_{2,m}(2) \\ \alpha_{2,m}^*(2) & -\alpha_{1,m}^*(2) \end{pmatrix} \cdot \begin{pmatrix} \mathcal{S}_1(2) \\ \mathcal{S}_2(2) \end{pmatrix} + \begin{pmatrix} \eta'_{1,m} \\ \eta'^*_{2,m} \end{pmatrix} \quad (7)$$

where $A[k]$ describes the kth element of vector A, and $S_i(j)$ is the ith super-symbol of User j. Note that $d = \lceil \frac{\delta_d}{T_s} \rceil$.

Equation (7) is essentially the same as (3) from which multiuser detection was derived. In (7), the effect of having two time-asynchronous transmissions is taken into account. Note that to cancel the interference from the second terminal, the receiver does not need to know the sampling error of the second terminal. As is evident from (7), this is due to the fact that the imperfectly sampled interference signal has an Alamouti structure independent of the sampling error ϵ. It is given that the samples from the extension of super-symbols are available at the receiver. To this end, no other transmission should take place in a distance of l symbol durations from each side of the packet. The SIFS[1] specified in the IEEE 802.11 standard provides this guard interval around the packets. Therefore, the MPR method in PHY introduces no transmission time overhead. For a case in which the packet that arrived second is to be decoded and the interference from the packet arrived earlier is to be canceled, the first few extension samples may not be available at the receiver. The solution is to first detect the earlier packet and then reconstruct the extension samples knowing the time delay between the two packets and channel coefficients [5]. In order to manage the available space, the details of this reconstruction are not provided.

Fig. 4 compares the BER performance of our asynchronous transmission method and that of the synchronous array processing method of [12]. In this figure, the synchronization error ϵ is picked randomly, and the average BER over a uniform distribution of ϵ is reported. From Fig. 4, it is clearly observed that the performance of our new asynchronous transmission method is very close to that of the synchronous method in [12] and provides a diversity order of 2.

C. Frequency Asynchrony

Having two physically separated radios at the exact same central frequency is practically impossible, and distributed radios always have different central frequencies. Hence, there is always a frequency offset δf between the central frequencies of transmitting and receiving radios. This frequency offset introduces a cumulative phase shift to the samples of the received signal. Consider a simple system of two time-synchronous single antenna terminals, with frequency offset δf. The kth sample of the received signal would be

$$r_k = \alpha_k s_k e^{j2\pi k \delta f T_s} + \eta_k \quad (8)$$

which translates to a linearly increasing phase shift over the samples of a packet.

When there are several transmitters, the ith terminal will have a frequency offset of δf_i. Taking into account the terminals' frequency offset, the folding process is modified, and the phase difference of the folded part is compensated to recreate a continuous linearly increasing phase shift for the interference. Accordingly, (7) is modified to

$$\begin{pmatrix} R_{1,m}[k] \\ R_{2,m}[k] \end{pmatrix} = \begin{pmatrix} 1 & 0 \\ 0 & e^{(j2\pi\Delta_1)} \end{pmatrix} \begin{pmatrix} S_1(1)[k] & S_2(1)[k] \\ -S_2^*(1)[k] & S_1^*(1)[k] \end{pmatrix} \cdot \begin{pmatrix} \alpha_{1,m}(1)e^{(j2\pi\delta_1)} \\ \alpha_{2,m}(1)e^{(j2\pi\delta_1)} \end{pmatrix} + \begin{pmatrix} 1 & 0 \\ 0 & e^{(j2\pi\Delta_2)} \end{pmatrix} \begin{pmatrix} \mathcal{S}_1(2)[k] & \mathcal{S}_2(2)[k] \\ -\mathcal{S}_2^*(2)[k] & \mathcal{S}_1^*(2)[k] \end{pmatrix} \cdot \begin{pmatrix} \alpha_{1,m}(2)e^{(j2\pi\delta_2)} \\ \alpha_{2,m}(2)e^{(j2\pi\delta_2)} \end{pmatrix} + \begin{pmatrix} \eta_{1,m} \\ \eta_{2,m} \end{pmatrix} \quad (9)$$

where $\Delta_i = M\delta f_i T_s$, $\delta_1 = k\delta f_1 T_s$ and $\delta_2 = (k-d-l)\delta f_2 T_s$.

Equation (9) can be restructured, similar to (3), as

$$\begin{pmatrix} R_{1,m}[k] \\ R_{2,m}^*[k] \end{pmatrix} = \Omega_{1,m}^k \begin{pmatrix} S_1(1)[k] \\ S_2(1)[k] \end{pmatrix} + \Omega_{2,m}^l \begin{pmatrix} \mathcal{S}_1(2)[k] \\ \mathcal{S}_2(2)[k] \end{pmatrix} + \begin{pmatrix} \eta'_{1,m} \\ \eta'^*_{2,m} \end{pmatrix} \quad (10)$$

where

$$\Omega_{i,m}^k = \begin{pmatrix} 1 & 0 \\ 0 & e^{(j2\pi\Delta_i)} \end{pmatrix} \mathbf{A}_m^k(i)$$
$$\mathbf{A}_m^k(i) = \begin{pmatrix} \alpha_{1,m}(i)e^{(j2\pi\delta_i)} & \alpha_{2,m}(i)e^{(j2\pi\delta_i)} \\ \alpha_{2,m}^*(i)e^{(-j2\pi\delta_i)} & -\alpha_{1,m}^*(i)e^{(-j2\pi\delta_i)} \end{pmatrix}. \quad (11)$$

$\Omega_{i,m}^k$ is a multiple of a unitary matrix so that $\Omega_{i,m}^{k\mathrm{H}}\Omega_{i,m}^k = \mathbf{A}_m^{k\mathrm{H}}(i)\mathbf{A}_m^k(i) = (|\alpha_{1,m}(i)|^2 + |\alpha_{2,m}(i)|^2)\mathbf{I} = |\Omega_{i,m}^k|^2\mathbf{I}$.

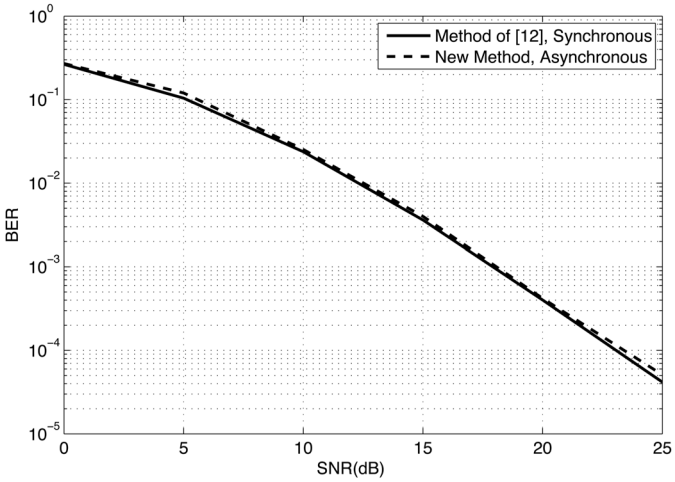

Fig. 4. Average performance comparison of our MPR method with an asynchronous transmission and the method of [12] using a synchronous transmission.

[1]"The SIFS is the time from the end of the last symbol of the previous frame to the beginning of the first symbol of the preamble of the subsequent frame as seen at the air interface" [14].

The next step is to cancel the interference from Terminal 2 to decode the data of Terminal 1. Similar to what was done for (4), we multiply each vector $R_m[k] = (R_{1,m}[k]R^*_{2,m}[k])^T$ with $\Omega^{k\mathrm{H}}_{2,m}$, divide it by $|\Omega^k_{2,m}|^2$, and subtract the result for $m = 1$ from that of $m = 2$. The following equation captures the results:

$$\frac{\Omega^{k\mathrm{H}}_{2,2}R^k_2}{\left|\Omega^k_{2,2}\right|^2} - \frac{\Omega^{k\mathrm{H}}_{2,1}R^k_1}{\left|\Omega^k_{2,1}\right|^2} = \left(\frac{\Omega^{k\mathrm{H}}_{2,2}\Omega^k_{1,2}}{\left|\Omega^k_{2,2}\right|^2} - \frac{\Omega^{k\mathrm{H}}_{2,1}\Omega^k_{1,1}}{\left|\Omega^k_{2,1}\right|^2}\right)\begin{pmatrix} S_1(1)[k] \\ S_2(1)[k] \end{pmatrix} + \begin{pmatrix} \eta''_{1,m} \\ \eta''_{2,m} \end{pmatrix}. \quad (12)$$

In (12), the matrix at the left side of the signal vector is a multiple of a unitary matrix. To prove this fact, it is enough to show that $\Omega^{k\mathrm{H}}_{2,m}\Omega^k_{1,m}$ is a unitary matrix. This is true due to the following:

$$\begin{aligned}
&\left(\Omega^{k\mathrm{H}}_{2,m}\Omega^k_{1,m}\right)^{\mathrm{H}}\left(\Omega^{k\mathrm{H}}_{2,m}\Omega^k_{1,m}\right) \\
&= \mathbf{A}^{k\mathrm{H}}_m(1)\begin{pmatrix} 1 & 0 \\ 0 & e^{(j2\pi(\Delta_2-\Delta_1))} \end{pmatrix}\mathbf{A}^k_m(2) \\
&\quad\times \mathbf{A}^{k\mathrm{H}}_m(2)\begin{pmatrix} 1 & 0 \\ 0 & e^{(-j2\pi(\Delta_2-\Delta_1))} \end{pmatrix}\mathbf{A}^k_m(1) \\
&= \left|\Omega^k_{2,m}\right|^2\mathbf{A}^{k\mathrm{H}}_m(1)\begin{pmatrix} 1 & 0 \\ 0 & e^{(j2\pi(\Delta_2-\Delta_1))} \end{pmatrix} \\
&\quad\times \begin{pmatrix} 1 & 0 \\ 0 & e^{(-j2\pi(\Delta_2-\Delta_1))} \end{pmatrix}\mathbf{A}^k_m(1) \\
&= \left|\Omega^k_{2,m}\right|^2\mathbf{A}^{k\mathrm{H}}_m(1)\mathbf{A}^k_m(1) = \left|\Omega^k_{2,m}\right|^2\left|\Omega^k_{1,m}\right|^2\mathbf{I}. \quad (13)
\end{aligned}$$

Knowing that this matrix is a multiple of a unitary matrix, decoding the data of Terminal 1 from (12) is straightforward.

D. Implementation Issues

We close this section by discussing some of the implementation issues. First, we note that this section assumes a perfect knowledge of channel coefficients, a perfect estimate of the delay, and a perfect estimate of the frequency offset between the two packets. There are algorithms to estimate all of the aforementioned parameters, but such algorithms obviously produce inaccurate results as the SNR of the received signal decreases. The gap between the theory and practice always affects the performance of implemented systems, and the implementation of the MPR algorithm is subject to the same effect. To implement our proposed MPR PHY, new algorithms might be required to enhance the accuracy of estimations. From the implementation standpoint, we note that our interference cancellation scheme does not require adding any major subsystem to the current transmission/reception modules of a system using Alamouti codes. At the transmitter, the coding block can be easily modified to accept super-symbols instead of standard symbols. A typical decoder has all required modules for estimating channel coefficients, frequency offsets, and sampling offsets. We need to estimate the delay between the two received signals. The latter quantity can be estimated using a correlator module that correlates the received signal to the known preamble. An IEEE 802.11 receiver already has a correlator module. A simple threshold processing of the output of this correlator can provide the time offset between the two packets [5]. Furthermore, the folding process only needs to access the memory and perform additions.

The elements of the $A^k_m(i)$ and $\Omega^k_{i,m}$ matrices in (11) can be calculated by feeding channel coefficient estimates to a derotator module [19]. Finally, the interference cancellation scheme of (12) requires complex conjugations, complex multiplications, and real divisions. After performing interference cancellation, an array processing operation similar to that of the Alamouti decoder is required in order to detect the transmitted data from the interference-free signal. No matrix inversion is required for this part, and the only needed operations are complex addition and complex multiplication.

III. MAC Algorithm

We open this section by noting that the use of MPR-aware MAC design methodologies does not affect the existing trade space of deterministic versus random access MAC algorithms. In fact, MPR-aware MAC design is affected by the characteristics of the utilized MAC algorithm. While scheduled designs require a central scheduler and signaling overhead to keep all nodes synchronized, random access methods have little signaling overhead at the cost of stimulating undesired collision effects. Thus, upgrading scheduled MAC algorithms such as TDMA, FDMA, and OFDMA to handle MPR is rather straightforward. The requirement is to assign one resource, i.e., time slot, or frequency band to more than one user. This process can be optimized by assigning resources to users based on their channel condition, QoS requirements, etc. Examples of such algorithms can be found in LTE MU-MIMO [17] and WiMAX collaborative MIMO [20]. Contrary to the case of deterministic MAC algorithms, incorporating MPR-awareness into the functionality of random access MAC algorithms such as CSMA is not straightforward due to the randomness characterizing access to channel resources. In this section, we design a CSMA-based MPR-aware MAC by making minimal essential modifications to the MAC algorithm of the IEEE 802.11 standard. We note that our goal is to design a practical and backward-compatible MPR-aware random access MAC without addressing any of the existing optimization trades. It is well known that the throughput performance of CSMA deteriorates rapidly as the network load increases. While modifications such as adding RTS/CTS signals and backoff mechanisms attempt at avoiding collisions and limiting bandwidth and time wastage, the resulting performance still vanishes as the number of nodes in the network increases and collisions dominate the performance.

In the case of two-antenna nodes and two-antenna APs, an AP can only detect two simultaneous transmissions, and receiving more than two simultaneous packets is treated as a collision. Therefore, the MPR-aware MAC must allow for as many double simultaneous information-exchange scenarios as possible and prevent higher than double transmission (collision) scenarios. MPR-aware MAC algorithms usually try to convert double collisions to multiple packet transmissions. Furthermore, such algorithms are usually designed for networks without hidden terminals. In this paper, we will introduce an MPR-aware MAC algorithm that increases the number of multiple packet transmissions by opening a waiting time window at the receiver and also

works for networks with hidden terminals. The latter is done by setting the parameter t_{w} as discussed below.

In the IEEE 802.11 standard, RTS messages are used by a transmitter to inform its target receiver of its intention to send data. A receiver responds with a CTS message if it is ready to receive that data.

In our MPR-aware MAC, RTS and CTS messages have the same functionality. In WLANs, all terminals communicate with the AP. Therefore, all multipackets received at the PHY of the AP can be decoded and are forwarded to higher layers. When the AP receives multiple packets, it has to be able to inform all corresponding transmitters that their packets have been received successfully. In the RTS/CTS handshake, the AP confirms the reception of packets twice, once via a CTS message when the RTS packet is received and once via an ACK message when the data packet is received. The same applies to our proposed MPR-aware MAC. Therefore, CTS/ACK frames are expanded by 6 B for the new receiver address field in order to target two nodes.

We introduce a waiting time of t_{w} at the receiver, which is the maximum tolerable time difference between the arriving RTS messages. In other words, when a receiver detects the beginning of an RTS packet, it opens a window of size t_{w} and searches for the beginning of any other RTS messages received in that time window. All double RTS messages reaching the receiver with a time difference less than t_{w} can be detected, and those with a larger time difference will be dropped, i.e., collision. On the other end, the transmitter increases the timeout for the RTS packet by adding t_{w} to the timeout duration of RTS messages in IEEE 802.11. While packet timeouts are not specified in IEEE 802.11 standard, a value of $\mathrm{EIFS}_{802.11} = \mathrm{SIFS} + \mathrm{CTS} + \mathrm{DIFS}$ is usually used for RTS packets. Therefore, $\mathrm{RTStimeout}_{\mathrm{MPR}} = \mathrm{EIFS}_{802.11} + t_w$.

In IEEE 802.11, a virtual channel sensing algorithm is used that forces nodes to hear an RTS message and to set their NAV timer to avoid collision with the ongoing transmission. In our MPR-aware MAC and for the purpose of encouraging multiple transmissions, the reception of two RTS messages in a node activates the virtual channel sensing process as opposed to setting up the NAV table, which is the result of receiving a single RTS message. We also note that the existence or lack of hidden terminals in a WLAN does not impact the algorithm in one way or another.

It is important to note that the only overhead introduced by our MPR-aware MAC algorithm is the extra receiver address field in the CTS and ACK messages, the waiting time at the AP, and the corresponding increase in the timeout value of RTS packets. In heavily loaded networks, this overhead is easily compensated for by multiple packet transmissions.

The AP can detect all pairs of RTS packets that are at most t_{w} seconds apart. Hence, by increasing t_{w}, the receiver has a better chance of detecting two packets simultaneously, in turn allowing more packets to transit within the network and increasing network throughput.

When two RTS packets are detected at the AP, a CTS packet will ask the corresponding transmitters to send their data packets. Both terminals receive the CTS packet at approximately the same time with a variation caused by the propagation delay. To facilitate synchronization at the AP, the terminals will send their data packets with different delays. The terminal whose address appears first in the CTS waits for SIFS and transmits its data packet. The other terminal will send its data packet after 2SIFS. Therefore, the MPR overhead is mainly related to transmitting RTS packets.

A packet drop in any of the signaling phases is regarded as a failed transmission, and the corresponding transmitters go through with the retransmission process as they would do in IEEE 802.11. This includes the cases in which the CTS/ACK message is sent for two transmitters, but only one of them receives the CTS/ACK packet correctly, i.e., the loss is due to bit errors.

It is worth noting that the above MAC algorithm can be used with any MPR method capable of detecting asynchronous packets such as SIC. The MPR method introduced in Section II provides diversity and has a lower BER in comparison to other MPR methods consuming the same amount of power. To detect long data packets successfully, the detection method must support a sufficiently low BER, or else the MPR method may decrease network throughput.

For better understanding of how our MPR-aware MAC algorithm affects the network performance, an analytical study aimed at identifying the saturation throughput of a sample example is provided in Section IV.

Before moving to the discussion of Section IV, we provide a brief discussion related to the deterministic MAC algorithms. We note that in deterministic algorithms such as those used by LTE and WiMAX, there is no collision to resolve, but controlled MPR opportunities as users are assigned by a central AP to a specific time-slot and/or frequency band. The saturation throughput improvement for these scenarios is roughly equal to $2\frac{1-\mathrm{PER}_{\mathrm{MPR}}}{1-\mathrm{PER}}$, where $\mathrm{PER}_{\mathrm{MPR}}$ is the packet error rate for the MPR and PER is the packet error rate for the normal operation mode. While the MAC algorithm is independent of the MPR technique employed at the PHY layer, MAC scheduling might be affected by the MPR technique's performance in terms of error probability.

IV. Throughput Analysis

In this section, we analyze the throughput of the MPR-aware MAC for a special case of having two hidden terminals as transmitters. The analysis is based on the PHY design described in Section II and the MAC layer described in Section III.

Throughput analysis for networks with hidden terminals is a complicated task. Bianchi [21] analyzes the throughput of IEEE 802.11 in a one-hop network using a two-dimensional Markov chain model. In [22], the Markov chain is extended to a three-dimensional Markov chain for multihop networks. However, the calculation is not precise and ignores some characteristics of multihop *ad hoc* networks. In [23], the hidden terminal problem is examined more closely, and a more exact analysis is presented. Following the approach of the latter paper, we calculate the throughput of a network with two hidden nodes and a constant contention window (CCW) size. In a network with only two nodes and assuming the MPR-aware MAC works perfectly, all transmissions will become double successful transmissions with no collisions. Even if a variable contention window size

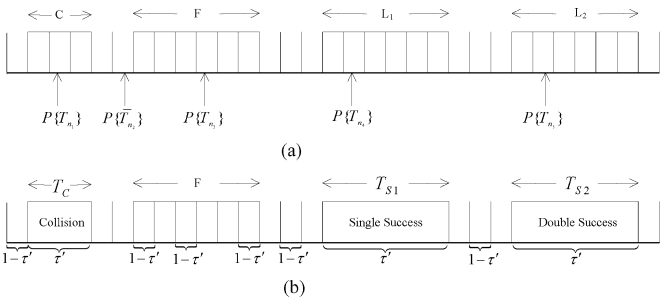

Fig. 5. Illustration of two different channel models around the transmitter [23]. (a) Model of the channel around the transmitter. (b) Discretization of the backoff period.

is chosen, an appropriate value of $t_{\rm W}$ can eliminate collisions. Without collision, the minimum contention window size will be chosen as the backoff window size, in effect representing the CCW size. The result of this analysis gives us an insight of how changing the value of $t_{\rm W}$ may affect performance. For our analytical model, we have the following set of assumptions.

1) Each terminal always has a packet to transmit (saturation traffic).
2) The operation of the PHY is perfect, and packets may be dropped only due to collisions not bit errors.
3) Time is normalized to a SlotTime θ duration.

As shown in Fig. 5, the main idea is to reconsider the time slot definition and in effect use two different definitions for time slots. Next and in order to calculate the probability of the occurrence of each time slot, a Markov chain as shown in Fig. 6 is formed. This Markov chain represents the backoff procedure employed by a node and illustrates how the backoff counter of that node changes its value. When the backoff counter reaches zero, the node starts transmitting. Each large circle represents a backoff counter value, and each small circle represents a freezing stage. Freezing stages last for F time slots as shown in Fig. 5. In Fig. 6, π_m is the steady state probability of being at state m, where the backoff counter value is m, and π_m^i is the steady-state probability of being in the ith freezing time slot while the backoff counter value is m. In order to calculate the transition probabilities of Fig. 6, channel state transitioning at the vicinity of a receiver is modeled by another Markov chain as illustrated in Fig. 7. A receiver may successfully receive a single packet in transit, successfully detect and receive two packets simultaneously in transit, or be unable to detect and receive two colliding packets simultaneously in transit. The Markov chain in Fig. 7 represents the aforementioned states of the channel at the vicinity of the receiver and the transitions from one state to another. As the last step, the exact values of the transitioning probabilities in Fig. 7 are calculated. In the sequel, the details of calculations are eliminated and only the main equations are presented.

While the analysis of this section is based on the analysis of [23], we make note of its major differences compared to that of [23]. First, the Markov chain representation of Fig. 6 is modified to capture the fact that the freezing probability varies as a function of the value of the backoff counter. The analysis of [23] ignores the fact that the probability of transmission for another transmitter increases after each inactive time slot. Second and as illustrated in Fig. 7, the analysis presented in this section considers the MPR scenario and as such has a set of channel states that are different from those of [23]. Consequently, the equations presented in this section are either partially different from those of [23] or completely new.

Fig. 5 illustrates different channel models and discretization used for analysis. Note that in this figure, C is the duration of a collision, F is the duration in which the backoff counter freezes the state, L_1 is the duration of a single successful transmission, and L_2 is the duration of a double successful transmission. Furthermore, $P\{T_n\}$, the probability that a node transmits in a time slot (illustrated in Fig. 5(a)) is a function of an intermediate transmission probability τ' [illustrated in Fig. 5(b)]. The relationship between these two probabilities is [23]

$$P\{T_n\} = \frac{\tau'}{\tau' + Q(1-\tau')} \tag{14}$$

where for the MPR-aware MAC, $Q = \frac{1}{P_{\rm S1}L_1 + P_{\rm S2}L_2 + pC}$. In addition, $P_{\rm S1}$, $P_{\rm S2}$, and p are conditional probabilities of the single successful transmission, double successful transmission, and collision, respectively.

To calculate τ', the Markov chain of Fig. 6 is used. Note that unlike the analysis of [23], the probabilities of going to freezing states are different for each stage of the backoff counter. As the backoff counter decrements its value, the probability of the other node starting a transmission grows up. Therefore, it is more probable to face freezing in the later stages of the counter in comparison to the earlier stages. Let $P_W(w)$ denote the conditional probability mass function for the freezing probabilities. Note that freezing happens only when the other node has a single successful transmission. From the analysis of the Markov chain, we have

$$\begin{aligned} \pi_m &= \frac{W-m}{W}\pi_0 \qquad m \in [1, W-1] \\ \pi_m^i &= P_W(m) P_{\rm S1} \pi_m \qquad m \in [1, W-1],\ i \in [1, F]. \end{aligned} \tag{15}$$

From (15), we get

$$\tau' = \pi_0 = \frac{2}{W + 1 + 2F/W \sum_{m=0}^{W-1} (W-m) P_W(m) P_{\rm S1}}. \tag{16}$$

The throughput of each node is the number of packets it can successfully transmit per slot. Each successful packet transmission is either a single transmission or a double transmission. If S_1 and S_2 denote the number of singly and doubly transmitted packets per slot, respectively, the throughput of each node S is

$$\begin{aligned} S_1 &= P\{T_n\} \cdot \frac{P_{\rm S1}L_1}{P_{\rm S1}L_1 + P_{\rm S2}L_2 + pC} \frac{1}{L_1} \\ S_2 &= P\{T_n\} \cdot \frac{P_{\rm S2}L_2}{P_{\rm S1}L_1 + P_{\rm S2}L_2 + pC} \frac{1}{L_2} \\ S &= S_1 + S_2 = P\{T_n\} \cdot (P_{\rm S1} + P_{\rm S2}) \cdot Q. \end{aligned} \tag{17}$$

To calculate the probabilities $P_{\rm S1}$, $P_{\rm S2}$, and p, an intermediate step is required. Suppose R is the receiver and A and B are two hidden transmitters. The transmission states for the channel around R can be modeled by a Markov chain as illustrated in Fig. 7. Transmissions observed by R have one of the following

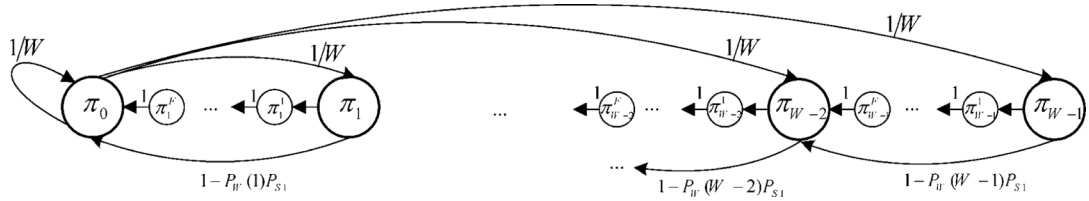

Fig. 6. Markov chain for CCW [23].

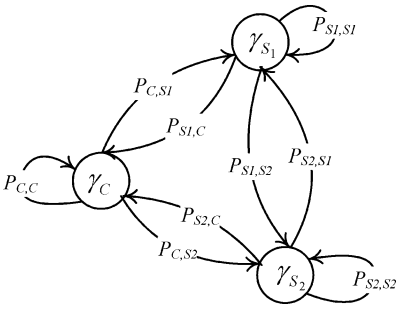

Fig. 7. Transmission states for the channel around the receiver.

states: collision $(\gamma_{\rm C})$, single transmission $(\gamma_{\rm S1})$, or double transmissions $(\gamma_{\rm S2})$. The steady-state probabilities of transmission states, $\gamma_{\rm C}$, $\gamma_{\rm S1}$, and $\gamma_{\rm S2}$ are easily calculated from Fig. 7 given the transition probabilities.

Let $N_{\rm Ca}$, $N_{\rm S1a}$, and $N_{\rm S2a}$ denote the steady-state values of the number of collisions, the number of single transmissions, and the number of double transmissions happening in the unit of time for Transmitter A, respectively. Recall that in the steady state, the number of single transmissions observed by R is twice the number observed by each transmitter. Furthermore, the number of collisions and double transmissions observed by A, B, and R are the same in the steady state. The following equations relate success and collision probabilities for Transmitters A and B to the steady-state probabilities of the transmission states of Receiver R:

$$\begin{aligned} p &= \frac{N_{\rm Ca}}{N_{\rm Ca}+N_{\rm S1a}+N_{\rm S2a}} \\ &= \frac{N_{\rm Ca}}{N_{\rm Ca}+2N_{\rm S1a}+N_{\rm S2a}} \cdot \frac{N_{\rm Ca}+2N_{\rm S1a}+N_{\rm S2a}}{N_{\rm Ca}+N_{\rm S1a}+N_{\rm S2a}} \\ &= \gamma_C \cdot \frac{1}{1-\gamma_{\rm S1}/2} \\ P_{\rm S1} &= \gamma_{\rm S1}/2 \cdot \frac{1}{1-\gamma_{\rm S1}/2} \\ P_{\rm S2} &= \gamma_{\rm S2} \cdot \frac{1}{1-\gamma_{\rm S1}/2}. \end{aligned} \tag{18}$$

New state transitions are visualized in Fig. 8, while the rest can be found in [23, Fig. 11]. In Fig. 8, X_A and X_B are the randomly chosen values for backoff counters of Transmitter A and Transmitter B, respectively. The distributions of X_A and X_B are uniform over $[0, 1, \ldots, W-1]$. The discrete random variable (DRV) Y is the offset, as a multiple of time-slot duration, between the transmission of the RTS packets when the result is a collision. H is a DRV representing the offset between two transmissions when the result is the detection of both packets. The DRV Z is the remaining number of backoff slots after a freezing phase. Note that from Fig. 8, the following transition states for Fig. 7 are given by:

$$\begin{aligned} P_{\rm C,S2} &= P\{|Y_{n-1}+X_A-X_B| \le D\} \\ P_{\rm S1,S2} &= P\{|X_B-Z_{n-1}| \le D\} \\ P_{\rm S2,S2} &= P\{|X_B-X_A| \le D\} \end{aligned} \tag{19}$$

where $D=[t_{\rm w}/\theta]$. It is worth noting that in a two-hidden-node configuration with $D > c = ({\rm RTS}+{\rm SIFS})/\theta$, there will be no collision in the transmissions and all transmissions are either single or double transmissions. Intuitively, choosing D close to contention window size W will maximize the throughput. This is due to the fact that under heavy traffic conditions, the offset of RTS messages coming from different nodes is less than W. Compared to single transmissions, bandwidth is used more efficiently for double transmissions. By choosing D close to W, most of the transmissions will be double transmissions.

The distributions of the DRVs Y, Z, and H are unknown. To calculate the corresponding probability mass functions (PMFs), note that the PMF of Z_{n-1} is the same as PMF of Z in the steady state. From Fig. 8, these distributions are recursively related. For example, from Fig. 8(a), (b), and (e)

$$\begin{aligned} H_n^{cs_2} &= Y_{n-1}+X_B-X_A \qquad \text{given } |Y_{n-1}+X_B-X_A| \le D \\ H_n^{s_1s_2} &= Z_{n-1}-X_A \qquad \text{given } |Z_{n-1}-X_A| \le D \\ H_n^{s_2s_2} &= X_B-X_A \qquad \text{given } |X_B-X_A| \le D. \end{aligned} \tag{20}$$

Note that in (20), the conditional distribution of $H_n^{s_2s_2}$ is independent of index n, while the conditional distribution of $H_n^{cs_2}$ and $H_n^{s_1s_2}$ are recursively related to the distribution of Y_{n-1} and Z_{n-1}. It is easy to see that the unconditional distribution of H is given by

$$\begin{aligned} P_H(k) = {} & P_{H^{s_1s_2}}(k) \cdot \Pr\left\{{\rm succ}_{n-1}^1 \,|\, {\rm succ}_n^2\right\} \\ & + P_{H^{s_2s_2}}(k) \cdot \Pr\left\{{\rm succ}_{n-1}^2 \,|\, {\rm succ}_n^2\right\} \\ & + P_{H^{cs_2}}(k) \cdot \Pr\left\{{\rm coll}_{n-1} \,|\, {\rm succ}_n^2\right\} \end{aligned} \tag{21}$$

where, for example, $\Pr\{{\rm succ}_{n-1}^1 \,|\, {\rm succ}_n^2\} = \Pr\{{\rm succ}_n^2 \,|\, {\rm succ}_{n-1}^1\} \cdot \frac{\Pr\{{\rm succ}_{n-1}^1\}}{\Pr\{{\rm succ}_n^2\}} = P_{S1,S2} \cdot \frac{P_{S1}}{P_{S2}}$ is the probability of having single success in the previous transmission given that the current transmission is a double success.

The PMFs of DRVs Z, Y, and H and the transition probabilities can be calculated in an iterative process such that a randomly chosen PMF is associated with each of the DRVs and transition probabilities are assigned random values in the initial state. In each step, the transition probabilities and the PMFs are refined using Fig. 8 and recursive equations such as (20) and (21). The

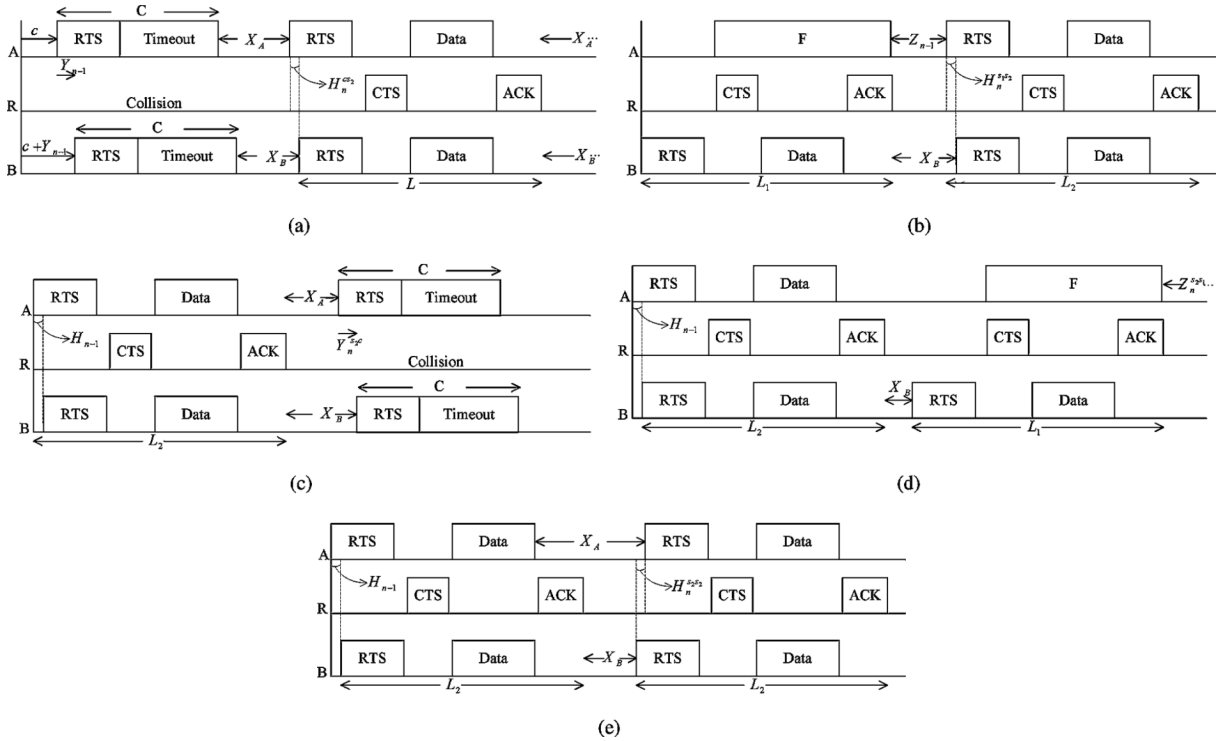

Fig. 8. Illustration of transitioning among different system states. (a) Collision to MPR. (b) SPR to MPR. (c) MPR to collision. (d) MPR to SPR. (e) MPR to MPR.

iterative process ends when it reaches the desired accuracy in a transition probability.

At last, note that the distribution of Z is the same as the conditional probability of freezing in Fig. 6, i.e., $P_W(w) = P_Z(w-1)$. Having identified all required elements of (17), the throughput per node of the two-hidden-node configuration is calculated.

V. Numerical Results

In this section, we study the saturation throughput of our proposed MPR PHY/MAC algorithm in comparison to the traditional IEEE 802.11 over a WLAN. We rely on Network Simulator (NS-2) as our discrete event simulation tool of interest. As discussed in [6], accurate implementation of the PHY in real time for network simulations is a time-consuming task. In order to address the latter problem, offline approximation approaches can be utilized as alternatives to real-time bit-level simulations because they can be run in a considerably shorter actual simulation period. Therefore, we separately simulated the MIMO transmission and interference cancellation methods using MATLAB. This led to forming tables of the average PER for different packet types and various values of SNR. The averaging was performed on different channel conditions and interference power levels. We used the average PER to drop arriving packets in MAC by generating a Bernoulli random variable with parameter p equal to the corresponding PER for each packet.

In the first three simulation scenarios, there is only one AP. The coverage area of the AP as well as that of the nodes are set to 200 m. Three simulation scenarios are considered. In the first scenario, there are only two nodes in the coverage area of the AP, and they are hidden from each other. This scenario is used to evaluate the analytical results and also study some basic

TABLE I
General Parameter Settings of Our Experimental Studies

SIFS	10μs
SlotTime(θ)	20μs
DIFS	SIFS+2SlotTime
MAC header	224
PHY header	192
RTS	160+PHY header
CTS	112+(48)+PHY header
ACK	112+(48)+PHY header
EIFS	SIFS+CTS+DIFS
Data (L)	$\in \{512, 1024\} \times 8$
Data Rate	2Mbps
Basic Rate	1Mbps

properties of the new MPR-aware MAC. The topology of the second scenario consists of N nodes placed on a circle around the AP such that each and every node in the network faces exactly h hidden nodes. In the third scenario, N nodes are placed randomly in a circular area around the AP such that the number of hidden terminals varies in the network, but on average $E(h)$ terminals are hidden from a node in the network. Other parameters are set according to Table I. Note that in the rest of this section, h is the number of hidden terminals in the second scenario and $E(h)$ is the average number of hidden terminals per node in the third scenario. Furthermore, t_{w} is measured as a multiple of time slots.

The topology used for the fourth simulation scenario covers a case in which there are two hidden APs. Fig. 9 shows the topology used in this experiment. The dashed lines represent the coverage area of the APs. In this scenario, each client communicates with the nearest AP.

Fig. 10 illustrates the results of simulation and analysis for the first scenario. The throughput is calculated for different packet

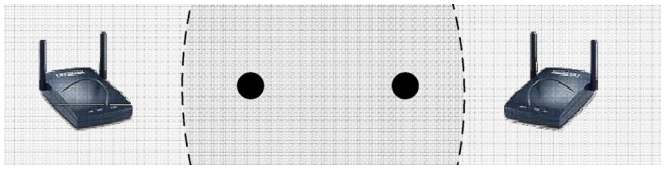

Fig. 9. Topology with hidden APs (black circles are representing clients).

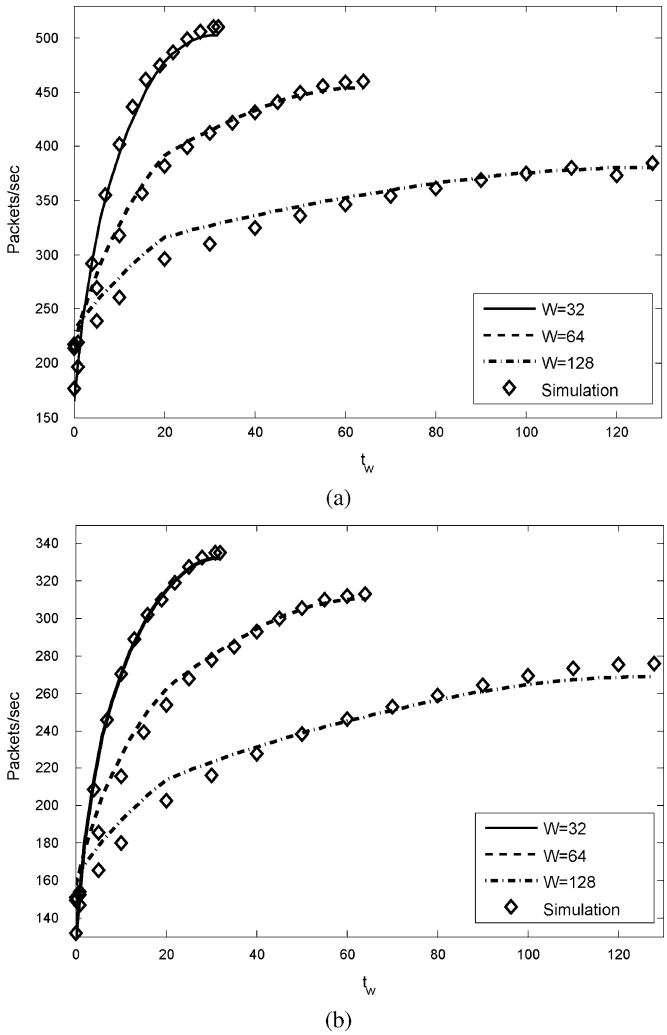

Fig. 10. Measurement of throughput of the first simulation scenario with (a) $L = 512$ B and (b) $L = 1024$ B.

lengths and contention window sizes (W). The important observation is that the analytical results match those of the simulation.

Note that increasing the waiting time beyond the contention window size will not change the throughput in this scenario. Below the contention window size, increasing the waiting time constantly increases the throughput as the result of increasing the number of double-packet transmissions. In the case of having two transmitters, for $t_{\rm w}$ longer than an RTS packet transmission time, i.e., $t_{\rm w} > 20$, no double-packet transmission is subject to a collision. Hence, slope changes are observed in the throughput curves of Fig. 10. Increasing the contention window size widens the range of offsets between transmissions

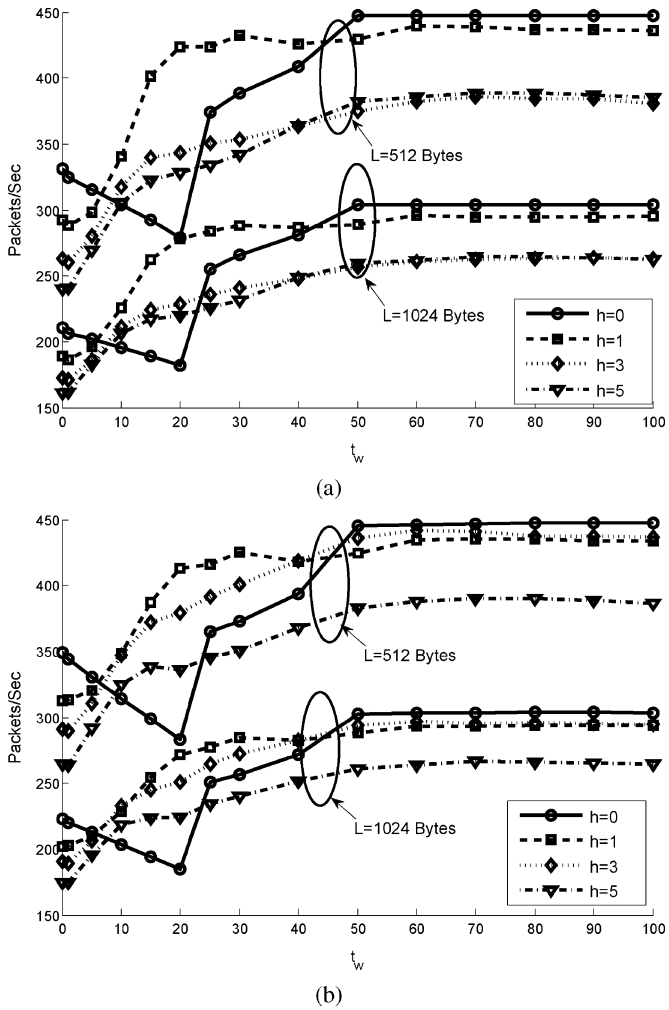

Fig. 11. Network throughput of the second simulation scenario for a case in which (a) 10 and (b) 20 terminals exist.

of the two transmitters. Therefore, the slope of the throughput curve decreases as the result of increasing W.

Simulation results of the second scenario are plotted in Fig. 11 for different packet lengths and different numbers of hidden terminals. In this set of simulations, the minimum contention window size $(\mathrm{CW}_{\min})$ and the maximum contention window size $(\mathrm{CW}_{\max})$ are set as defined in the IEEE 802.11 standard for direct sequence spread spectrum (DSSS) PHY, which is $\mathrm{CW}_{\min} = 32$ and $\mathrm{CW}_{\max} = 2^m \mathrm{CW}_{\min}$, where $m = 5$ is the number of backoff stages. Note that the parameter $t_{\rm w}$ is introduced in our new MAC and does not exist in IEEE 802.11. Therefore, the performance of IEEE 802.11 is reported in Table II for each curve in Fig. 11. All of the curves in Fig. 11 are following similar patterns except in the case of having no hidden terminals in the network. For $h = 0$, increasing the waiting time for RTS packets while $t_{\rm w} < 20$ decreases the throughput and then sharply increases the throughput. Since nodes do not begin a transmission while they sense a busy channel and further all nodes can hear each others transmissions, waiting for a second RTS message with $t_{\rm w} < 20$ only increases the overhead of the transmission without resulting in any multipacket transmissions. Ignoring this misbehavior

TABLE II
THROUGHPUT OF IEEE 802.11 FOR THE SECOND SCENARIO

N	L	$h=0$	$h=1$	$h=3$	$h=5$
10	512 B	274	269	257	234
	1024 B	176	173	168	157
20	512 B	269	258	250	242
	1024 B	171	169	165	161

TABLE III
THROUGHPUT OF IEEE 802.11 WITH RTS/CTS TURNED OFF AND NO HIDDEN TERMINALS

N	L	$h=0$	N	$h=0$
10	512 B	289	20	274
	1024 B	173		159

and increasing the waiting time results in first increasing and then slowly decreasing the throughput. The best throughput can be achieved around $t_{\rm w} = 60$ time slots, independent of the topology of the network and packet length. Therefore, the best value of the design parameter $t_{\rm w}$ can be calculated offline. Comparing the simulation results of Fig. 11 to those presented in Table II shows a considerable enhancement in the network throughput as the result of using the MPR-aware MAC. In networks with no hidden terminals, turning off the RTS/CTS messaging in IEEE 802.11 may still improve the network throughput. As reported in Table III, the results for such networks reveal that the MPR-aware MAC outperforms IEEE 802.11 even in the latter case.

Fig. 12 illustrates the simulation results for a network of randomly positioned nodes with an average number of hidden nodes as described for the third scenario. Here, we set a minimum contention window size of $\mathrm{CW}_{\min} = 32$ and five backoff stages, i.e., $m = 5$. In comparison to the results of Fig. 11, one observes similar trends in response to increasing the waiting time, i.e., $t_{\rm w}$ in both scenarios. Similar to the second scenario, setting $t_{\rm w} = 60$ is a reasonable choice for waiting time to achieve the maximum throughput gain independent of the network topology, packet length, and the number of users. The throughput of IEEE 802.11 for this scenario is reported in Table IV. Comparing the throughput curves of MPR-aware MAC and the throughput of IEEE 802.11 network reveals that the MPR-aware MAC always improves the throughput no matter what the waiting time value is. In addition, it can improve the throughput up to 80% depending on the choice of waiting time and the network topology.

The last simulation scenario is performed to measure the downlink throughput of the network in Fig. 9. The result of the simulation for this network topology is illustrated in Fig. 13. Compared to IEEE 802.11, the throughput of the MPR-aware MAC is 94% better than that of IEEE 802.11. The throughput improvement in the downlink scenario is considerable and illustrates the MPR-aware MAC potential to solve the hidden-AP problem in deployed IEEE 802.11 networks. Further study of downlink performance for MPR-aware MAC is out of the scope of this paper and is considered as a future extension of this work.

The effects of having different window sizes is studied in Fig. 14. In Fig. 14(a), $\mathrm{CW}_{\min} = 32$ is constant, and m varies from 0 to 5. Increasing m randomizes the transmission times

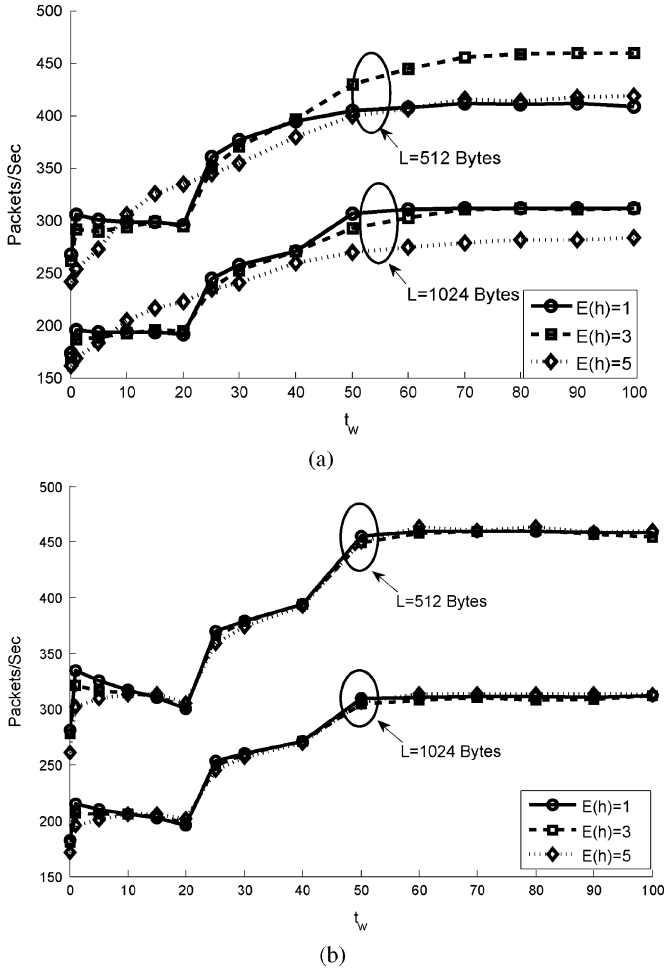

Fig. 12. Network throughput of the third simulation scenario for a case in which (a) 10 and (b) 20 terminals exist.

TABLE IV
THROUGHPUT OF IEEE 802.11 FOR THE THIRD SCENARIO

N	L	$E(h)=1$	$E(h)=3$	$E(h)=5$
10	512 B	268	267	245
	1024 B	173	172	162
20	512 B	261	259	255
	1024 B	170	169	168

over wider ranges and reduces collisions for IEEE 802.11. IEEE 802.11 performs better for larger values of m. On the other hand, the MPR-aware MAC has a constant throughput over different values of m, and its performance is independent of the maximum contention window size. In Fig. 14(b), $\mathrm{CW}_{\max} = 512$ is constant, and m varies from 1 to 5. In contrast to the last case, IEEE 802.11 has a relatively constant performance as $\mathrm{CW}_{\min}$ changes. Since the number of hidden terminals is high, i.e., half of the total number of active nodes, each transmission most probably faces a collision. Therefore, nodes increase their contention window sizes till they reach $\mathrm{CW}_{\max}$ and, as such, the performance does not change with variations of the initial window size. To the contrary, the MPR-aware MAC's performance differs depending on the initial window size. We observe that a smaller value of the minimum contention window size results in a better performance for the MPR-aware MAC. This is because most collisions

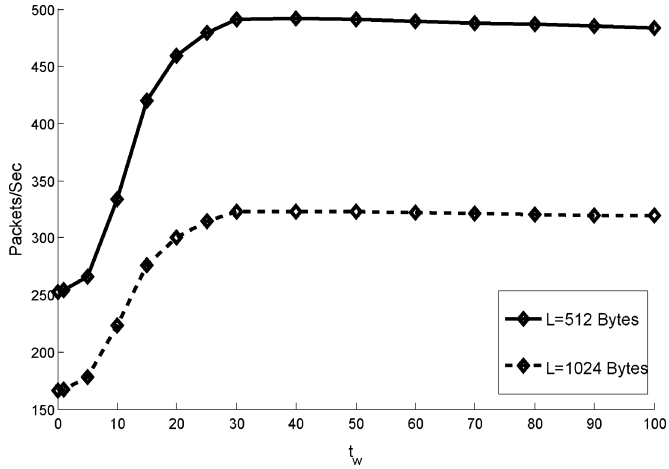

Fig. 13. Downlink throughput of the network in Fig. 9. IEEE 802.11 throughput is 253 and 166 for $L = 512$ B and $L = 1024$ B, respectively.

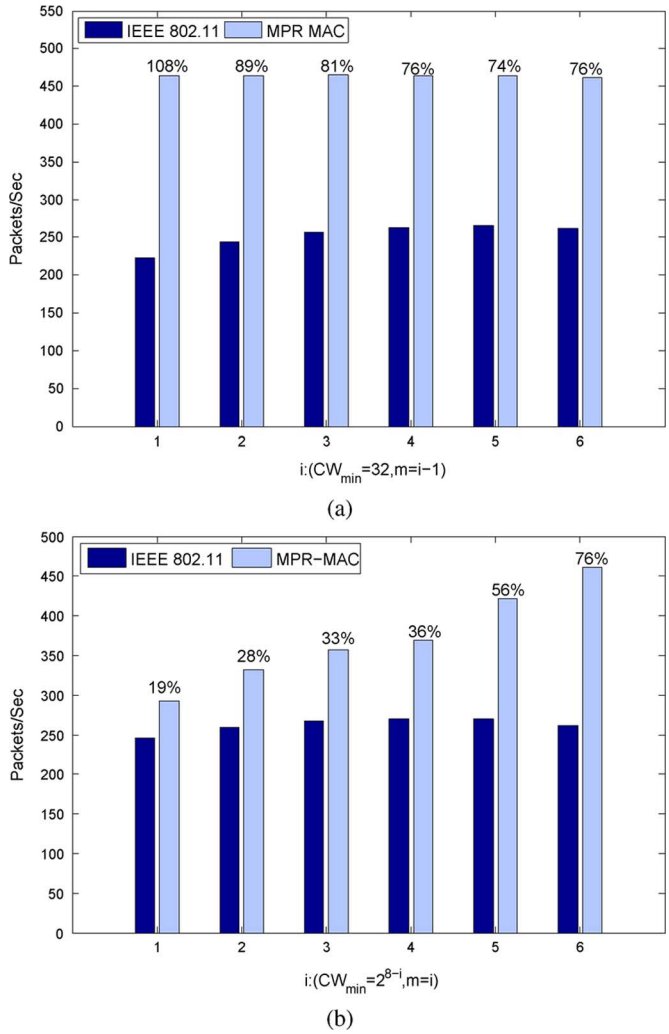

Fig. 14. Performance profiling results of the MPR-aware MAC algorithm for different values of window size in a network consisting of $N = 20$ terminals and $E(h) = 1$, where (a) $\mathrm{CW}_{\min}$ is constant and (b) $\mathrm{CW}_{\max}$ is constant.

are transformed to double successful transmissions for the MPR-aware MAC, and hence window sizes are kept at their smallest values. Smaller contention window sizes imply more double transmissions, and therefore higher throughput gains for the MPR-aware MAC.

VI. Conclusion

In this paper, we proposed a cross-layer PHY-MAC MPR method based on the use of space–time coding techniques. Previously proposed MPR methods based on space–time coding were mainly designed for perfectly synchronized transmission scenarios, and their performance was shown to be sensitive to transmission asynchrony. We proposed an STC-based MPR transmission and detection method that is tolerant to both time and frequency asynchrony. We showed that, in asynchronous transmissions, our proposed method provides the same diversity gain as that associated with previously proposed synchronous methods. Although we have presented our scheme for users with two transmit antennas, in general, orthogonal STBCs and quasi-orthogonal STBCs can be used for more than two antennas [10]. Similarly, the proposed interference cancellation method can be extended to more than two users with more than two antennas [13]. For example, if J users communicate with N antenna receivers, the array processing technique presented in [13] provides each user with a receive diversity of $N - J + 1$. The scheme in [13] is designed to detect synchronous packets. However, designing an asynchronous scheme based on the ideas presented in this paper is straightforward.

In support of the MPR-based PHY design, we also described our MAC design as an extension of IEEE 802.11 with RTS/CTS signaling capable of operating in WLANs with and without hidden terminals. Our MPR-aware MAC algorithm operated by widening its acceptance duration in the receiving side in order to allow for accepting a larger number of double incoming RTS messages. The MAC algorithm can be readily generalized to support reception of more than two simultaneous packets.

We studied the tradeoff related to the choice of this widened acceptance duration. We observed that while the use of a longer waiting time increased the probability of collisions for more than two RTS messages, such increase in the waiting time duration also resulted in a greater chance of success for double transmissions. Simulation results consistently showed a significant performance improvement compared to the baseline of IEEE 802.11 standard. Besides focusing on the problem of designing an MPR-aware MAC algorithm for ad hoc networks, our future work considers studying new scheduling policies for MPR-aware MAC algorithms maximizing the chance of having double and multiple collisions instead of avoiding them. Furthermore, MPR-aware MAC can be potentially used to solve hidden-AP problems in networks with dominant downlink traffic. Examining the behavior of the MPR-aware MAC in networks with multiple overlapping cells and different traffic patterns as well as adopting its design for such scenarios of operation is the subject of our ongoing research work.

References

[1] V. Srivastava and M. Motani, "Cross-layer design: A survey and the road ahead," *IEEE Commun. Mag.*, vol. 43, no. 12, pp. 112–119, Dec. 2005.

[2] A. Li, M. Wang, X. Li, and H. Kayama, "A cross-layer design on the basis of multiple packet reception in asynchronous wireless network," in *Proc. IEEE ICC*, Jun. 2007, pp. 3477–3484.

[3] N. Santhapuri, R. R. Choudhury, J. Manweiler, S. Nelakuduti, S. Sen, and K. Munagala, "Message in message (MIM): A case for reordering transmissions in wireless networks," in *Proc. HotNets*, Oct. 2008, pp. 1–6.

[4] J. Manweiler, N. Santhapuri, S. Sen, R. R. Choudhury, S. Nelakuditi, and K. Munagala, "Order matters: Transmission reordering in wireless networks," in *Proc. ACM MobiCom*, Sep. 2009, pp. 61–72.

[5] S. Gollakota and D. Katabi, "Zigzag decoding: Combating hidden terminals in wireless networks," in *Proc. ACM SIGCOMM*, Oct. 2008, vol. 38, no. 4, pp. 159–170.

[6] M. Zorzi, J. Zeidler, A. Anderson, B. Rao, J. Proakis, A. Swindlehurst, M. Jensen, and S. Krishnamurthy, "Cross-layer issues in MAC protocol design for MIMO ad hoc networks," *IEEE Trans. Wireless Commun.*, vol. 13, no. 4, pp. 62–76, Aug. 2006.

[7] P. X. Zheng, Y. J. Zhang, and S. C. Liew, "Multipacket reception in wireless local area networks," in *Proc. IEEE ICC*, Jun. 2006, pp. 3670–3675.

[8] P. Casari, M. Levorato, and M. Zorzi, "MAC/PHY cross-layer design of MIMO ad hoc networks with layered multiuser detection," *IEEE Trans. Wireless Commun.*, vol. 7, no. 11, pp. 4596–4607, Nov. 2008.

[9] W. L. Huang, K. Letaief, and Y. J. Zhang, "Cross-layer multi-packet reception based medium access control and resource allocation for space-time coded MIMO/OFDM," *IEEE Trans. Wireless Commun.*, vol. 7, no. 9, pp. 3372–3384, Sep. 2008.

[10] H. Jafarkhani, *Space-Time Coding: Theory and Practice*. Cambridge, U.K.: Cambridge Univ. Press, 2005.

[11] P. Wolniansky, G. Foschini, G. Golden, and R. Valenzuela, "V-BLAST: An architecture for realizing very high data rates over the rich-scattering wireless channel," in *Proc. ISSSE*, Sep. 1998, pp. 295–300.

[12] A. Naguib, N. Seshadri, and A. Calderbank, "Applications of space-time block codes and interference suppression for high capacity and high data rate wireless systems," in *Proc. 32nd Asilomar Conf. Signals, Syst. Comput.*, Nov. 1998, vol. 2, pp. 1803–1810.

[13] J. Kazemitabar and H. Jafarkhani, "Multiuser interference cancellation and detection for users with more than two transmit antennas," *IEEE Trans. Commun.*, vol. 56, no. 4, pp. 574–583, Apr. 2008.

[14] *IEEE 802.11 Standard—Part 11: Wireless LAN Medium Access Control (MAC) and Physical Layer (PHY) Specifications*, IEEE 802.11, Jan. 2007.

[15] H. Guo, H. Hu, and Y. Zhang, "A high-throughput random access protocol for multiuser mimo systems," *EURASIP Res. Lett. Commun.*, vol. 2008, pp. 5:1–5:5, Jan. 2008.

[16] N. Freris and P. Kumar, "Fundamental limits on synchronization of affine clocks in networks," in *Proc. 46th IEEE CDC*, Dec. 2007, pp. 921–926.

[17] S. Sesia, I. Toufik, and M. Baker, *LTE, The UMTS Long Term Evolution: From Theory to Practice*. Hoboken, NJ: Wiley, 2009.

[18] S. Alamouti, "A simple transmit diversity technique for wireless communications," *IEEE J. Sel. Areas Commun.*, vol. 16, no. 8, pp. 1451–1458, Oct. 1998.

[19] T.-D. Chiueh and P.-Y. Tsai, *OFDM Baseband Receiver Design for Wireless Communications*. Hoboken, NJ: Wiley, 2007.

[20] J. G. Andrews, A. Ghosh, and R. Muhamed, *Fundamentals of WiMAX: Understanding Broadband Wireless Networking*. Englewood Cliffs, NJ: Prentice-Hall, 2007.

[21] G. Bianchi, "Performance analysis of the IEEE 802.11 distributed coordination function," *IEEE J. Sel. Areas Commun.*, vol. 18, no. 3, pp. 535–547, Mar. 2000.

[22] J. He and H. K. Pung, "Performance modeling and evaluation of IEEE 802.11 distributed coordination function in multihop wireless networks," in *Proc. ICON*, Nov. 2004, pp. 73–79.

[23] A. Tsertou and D. I. Laurenson, "Revisiting the hidden terminal problem in a CSMA/CA wireless network," *IEEE Trans. Mobile Comput.*, vol. 7, no. 7, pp. 817–831, Jul. 2008.

Sanaz Barghi (S'09) received the B.S. and M.S. degrees in electrical engineering from Sharif University of Technology, Tehran, Iran, in 2005 and 2007, and is currently pursuing the Ph.D. degree in electrical engineering and computer science at the University of California, Irvine.

Her research interests include wireless communications and wireless networks.

Hamid Jafarkhani (S'86–M'89–SM'01–F'06) received the B.S. degree in electronics from Tehran University, Tehran, Iran, in 1989, and the M.S. and Ph.D. degrees in electrical engineering from the University of Maryland, College Park, in 1994 and 1997, respectively.

In 1997, he was a Senior Technical Staff Member with AT&T Laboratories–Research, Red Bank, NJ, and was later promoted to a Principal Technical Staff Member. He is currently a Chancellor's Professor with the Department of Electrical Engineering and Computer Science, University of California, Irvine (UCI), where he is also the Director of the Center for Pervasive Communications and Computing and the Conexant-Broadcom Endowed Chair. He is listed as a highly cited researcher at http://www.isihighlycited.com. According to Thomson Scientific, he is one of the top 10 most-cited researchers in the field of computer science during 1997–2007. He is the author of the book *Space-Time Coding: Theory and Practice* (Cambridge Univ. Press, 2005).

Dr. Jafarkhani was an Associate Editor for IEEE COMMUNICATIONS LETTERS from 2001 to 2005, an Editor for the IEEE TRANSACTIONS ON WIRELESS COMMUNICATIONS from 2002 to 2007, an Editor for the IEEE TRANSACTIONS ON COMMUNICATIONS from 2005 to 2007, and a Guest Editor of the Special Issue on MIMO-Optimized Transmission Systems for Delivering Data and Rich Content for the IEEE JOURNAL OF SELECTED TOPICS IN SIGNAL PROCESSING in 2008. Currently, he is an Area Editor for the IEEE TRANSACTIONS ON WIRELESS COMMUNICATIONS. He ranked first in the nationwide entrance examination of Iranian universities in 1984. He was a co-recipient of the American Division Award of the 1995 Texas Instruments DSP Solutions Challenge. He received the best paper award of ISWC in 2002 and an NSF Career Award in 2003. He received the UCI Distinguished Mid-Career Faculty Award for Research in 2006 and the School of Engineering Fariborz Maseeh Best Faculty Research Award in 2007. Also, he was a co-recipient of the 2006 IEEE Marconi Best Paper Award in Wireless Communications and the 2009 Best Paper Award of the *Journal of Communications and Networks*.

Homayoun Yousefi'zadeh (S'96–M'98–SM'06) received the B.S. degree from Sharif University of Technology, Tehran, Iran, in 1989, the M.S. degree from Amirkabir University of Technology, Tehran, Iran, in 1993, and the Ph.D. degree from the University of Southern California, Los Angeles, in 1997, all in electrical engineering.

He is currently an Associate Adjunct Professor with the Department of Electrical Engineering and Computer Science, University of California, Irvine. He is also a Consulting Scientist with the Boeing Company, Huntington Beach, CA. Most recently, he was the CTO of TierFleet, Inc., Irvine, CA, working on distributed database systems; a Senior Technical and Business Manager with Procom Technology, Irvine, CA, focusing on storage networking; and a Technical Consultant with NEC Electronics, Mountain View, CA, designing and implementing distributed client–server systems. He is the inventor of four patents.

Dr. Yousefi'zadeh served as the Chairperson of the Systems Management Workgroup of the Storage Networking Industry Association (SNIA) and as a member of the Scientific Advisory Board of the Integrated Media Services Center (IMSC), University of Southern of California. He is an editor of the IEEE TRANSACTIONS ON WIRELESS COMMUNICATIONS and the *Journal of Communications and Networks*. From 2005 to 2010, he was an Associate Editor of the IEEE COMMUNICATIONS LETTERS. From 2006 to 2010, he was an Editor of the *IEEE Wireless Communications Magazine*. He also served as the lead Guest Editor of the IEEE JOURNAL OF SELECTED TOPICS IN SIGNAL PROCESSING April 2008 issue. He serves regularly as a member of the Technical Program Committees of various IEEE Communications Society conferences including ICC, GLOBECOM, and WCNC. He is a recipient of the *Journal of Communications and Networks* 2009 Best Paper Award.